A study of the geometry and parameter dependence of vortex breakdown

M. C. Jones, K. Hourigan, and M. C. Thompson

Citation: Physics of Fluids (1994-present) **27**, 044102 (2015); doi: 10.1063/1.4916352
View online: http://dx.doi.org/10.1063/1.4916352
View Table of Contents: http://scitation.aip.org/content/aip/journal/pof2/27/4?ver=pdfcov
Published by the AIP Publishing

A study of the geometry and parameter dependence of vortex breakdown

M. C. Jones,[1,a)] K. Hourigan,[1,2] and M. C. Thompson[1]
[1]*Fluids Laboratory for Aeronautical and Industrial Research (FLAIR), Department of Mechanical and Aerospace Engineering, Monash University, Melbourne, Australia*
[2]*Laboratory for Biomedical Engineering, Monash University, Melbourne, Australia*

(Received 26 July 2014; accepted 3 March 2015; published online 3 April 2015)

The types of vortex breakdown observed in the torsionally driven cylinder (TDC) flow and in the flow through an open-ended pipe are compared. The connection between the various breakdown types is specifically addressed, and the differences in manifestation of breakdown are attributed to the different Reynolds number regimes involved. Here, in both cases, the Reynolds number is based on quantities associated with the vortex core immediately upstream of breakdown, rather than the more geometry-specific Reynolds number defined in the previous work. Thus, the relationship between the TDC flow and the flows observed in other, more open geometries, is clarified. The predominantly asymmetric breakdown observed in open high Reynolds number flows is replaced by a closed bubble form with decreasing Reynolds number in the TDC. Three-dimensional numerical simulations support this interpretation, showing that the 3D spiral type of breakdown is replaced by a TDC-type axisymmetric breakdown in an open pipe as the Reynolds number is reduced. The stability of the three-dimensional solutions indicates that spiral breakdown modes stabilise at lower Reynolds number, leading to an axisymmetric breakdown state as a stable evolved flow solution. © *2015 AIP Publishing LLC.* [http://dx.doi.org/10.1063/1.4916352]

I. INTRODUCTION

Recent years have seen an increasing interest in vortex breakdown, due to its association with highly manoeuvrable aircraft, which continue to adopt variants of the delta wing planform. Breakdown has long been associated with the highly swept delta planform of the F/A-18 leading-edge extension, for example, and the effect of breakdown for this aircraft, in particular, is well known: the unsteadiness downstream of breakdown leads to tail buffetting and hence increased fatigue. Some of the next generation of proposed unmanned combat air vehicles and micro-air vehicles also have a delta planform, often with lower sweep. Lower sweep results in an increased propensity toward the appearance of vortex breakdown. Since these aircraft will be capable of extreme manoeuvres where breakdown can manifest, the phenomenon must be considered as part of the aerodynamics of such wings (Gursul, Gordnier, and Visbal[1]).

Breakdown can also be observed in the swirling flow in a confined cylinder. The mixing properties of the flow in a confined cylinder have practical importance for cell culture and tissue engineering following initial experimental investigations,[2,3] computational studies,[4–10] and cell culture.[11] The structure and stability of the vortex breakdown bubble in such bioreactors has important implications for the rate of nutrient transfer and waste disposal, and whether the vortex breakdown bubble itself could be used as a "virtual reactor" in which constructs such as scaffolds could be placed or cells cultured.

The measures which have thus far been applied to control vortex breakdown have relied on manipulation of parameters that have long been known to influence breakdown. These parameters

[a)]Present address: Equos Research Co., Ltd., Anjo, Japan.

include the swirl level of the base vortical flow and the pressure gradient (up to a limit, high swirl and an adverse pressure gradient promote the onset of breakdown). One review of the progress made in breakdown control is Mitchell and Delery,[12] and research into control methods is continuing.[13–17] Despite the significant control demonstrated however, these methods appear not to have contributed to breakdown control in practice. The current solution for the F/A-18, for instance, is the placement of a vortex generator on the surface of the leading-edge extension to divert the vortex outboard of the vertical stabilizers, where breakdown when it does occur can do less harm.

In addition to studies of breakdown control, theoretical research has contributed much to the understanding of the mechanism for breakdown. It is now widely considered that breakdown results from the waveguide nature of vortical flows, as described by Benjamin.[18] In this context, breakdown has been associated with a point where the vortex core becomes capable of supporting upstream travelling disturbances. At this point, disturbances on the vortex core "pile up," resulting in expansion of the vortex, and eventually stagnation and the formation of a recirculation region in the case of the bubble form of breakdown. A description of this model is given by Randall and Leibovich.[19] The relationship between this mechanism and the stability of the flow is described in Wang and Rusak[20] and Rusak, Whiting, and Wang.[21] In addition, the generation of negative azimuthal vorticity has been shown to be a necessary condition for the onset of breakdown,[22,23] and Darmofal and Murman[24] described the generation of this negative azimuthal vorticity by disturbance trapping.

The description of a mechanism for breakdown is complicated by the fact that a number of different flow phenomena have been described as breakdown. The experimental study of a swirling jet by Billant, Chomaz, and Huerre[25] revealed both axisymmetric and asymmetric bubble and conical structures. Asymmetry was shown to occur at higher Reynolds number relative to the axisymmetric forms. A stability analysis[26] of this flow predicted the onset of a double helix structure at a swirl below that required for breakdown, and the double helix was observed in the experiments. However, the analysis could not predict the axisymmetric bubble mode also observed experimentally. In a later study,[27] the spiral form of breakdown, which is often observed downstream of the bubble form, was shown to be associated with a global instability in the wake of the axisymmetric bubble.[28]

In a study of more direct relevance to aeronautical flows, Rusak and Lamb[29] showed that breakdown onset over slender delta wings could be predicted from the swirl ratio of the leading-edge vortex. The linear stability and critical state analyses of Renac and Jacquin[30] indicated that for delta wings, disturbances upstream of breakdown are either damped or weakly amplified, and that downstream of breakdown, asymmetric modes are amplified. This supported the previous work that indicated a role for instability in the transition to asymmetric breakdown,[27] but not for the axisymmetric (bubble) mode.

In contrast to that work, studies of the mechanism for breakdown are generally conducted at much lower Reynolds numbers, and for very different geometries, compared with the typical flight regime for real aircraft. The behaviour of breakdown in simplified geometries at very low Reynolds number is significantly different to the behaviour observed over real wings. As discussed in Herrada and Fernandez-Feria[31] at low Reynolds number in the torsionally driven cylinder (TDC), the breakdown form is axisymmetric, but at higher Reynolds number (for example, over delta wings), breakdown is predominantly asymmetric. (Some observations of asymmetric breakdown in the TDC at low Reynolds number have been reported. Experiments and calculations have indicated that very slight asymmetries in the TDC geometry, i.e., very slight structural asymmetries, can lead to clearly asymmetric flows.[32,33] In addition, slight visualisation technique asymmetries, such as slight misalignments in dye injection[34] and dye diffusion[35] can lead to strongly asymmetric visualisations even for strictly symmetric flows. The onset of precession of the breakdown bubbles in the TDC has, however, been observed for high Reynolds numbers[36,37] and at cylinder aspect ratios above 3.3, asymmetry has also been observed.[38,39]

The different observations of breakdown in the low Reynolds number confined flows, and the high Reynolds number open flows, have caused some to question the relationship between the breakdowns observed in these different situations. Importantly, although there may be some degree of implicit understanding of the relationship between different breakdown states by experienced workers in the field, to the authors' knowledge, few papers have specifically addressed the reasons

for the different manifestations. The intention here is to directly address this issue, and both clarify and quantify the relationship between the various breakdown forms observed.

We suggest that the relationship between the TDC and open flows can be more easily understood using parameters that are more consistently related to the physical conditions leading to breakdown. In the current work, we directly compare the various flows which support breakdown using such parameters. Following this, we show how observations of symmetric breakdown in the TDC follow from the much lower effective Reynolds number of the TDC flow, as confirmed by the observation that reducing the Reynolds number in a pipe to a level similar to that in the TDC, the asymmetry in that geometry also disappears.

The analysis proceeds as follows:

1. The nature of the flows resulting in breakdown in open pipe and TDC geometries are compared initially by examining the flow upstream of breakdown.
2. More appropriate definitions of Reynolds number and swirl are proposed to allow more direct comparison of the TDC and open pipe flows.
3. In light of the above analysis, the variation in breakdown observations between geometries is discussed.
4. A final three-dimensional modelling exercise of a pipe flow at very low Reynolds number is used to confirm the main assertions.

II. NUMERICAL METHOD

Variants of spectral-element codes were used for the simulations. These codes have been extensively validated previously so only brief descriptions will be provided here, with further details found in the articles referenced.

A. Steady axisymmetric code

Steady axisymmetric flows were computed using an axisymmetric steady solver based on Newton iteration and enforcing continuity using the penalty approach.[40] Within each spectral element, the internal nodes are distributed based on the Gauss-Legendre-Lobatto quadrature points, with flow variables represented through tensor-product Lagrange polynomial expansions, and in turn GLL quadrature is used to evaluate the integrals from the application of the weighted residual method. The number of internal nodes can be chosen at runtime, allowing resolution studies to be conducted to verify the predictions are converged. This method has been previously applied to flows with vortex breakdown in Thompson and Hourigan.[32]

B. Spectral/spectral-element code

For the three-dimensional pipe calculations, a spectral/spectral-element method was used. The method is described in Thompson, Hourigan, and Sheridan[41] and a more detailed description of the formulation of the spectral-element method can be found in the study by Karniadakis and Triantafyllou.[42] The aim of the technique is to balance the superior convergence of higher-order global spectral methods with the ability to model a greater variety of geometries. For the pipe geometry considered here, solutions in an axial-radial plane can be obtained using a two-dimensional spectral element mesh. For each element, high-order Lagrangian polynomial interpolation is used to represent the spatial variation of the solution variables. The method is extended to three dimensions by the addition of a Fourier spectral decomposition in the azimuthal direction. Time integration is performed in three steps, accounting for convection, pressure, and diffusion terms. The third-order Adams-Bashforth method is employed for the convection equation, and the Crank-Nicholson scheme for the diffusion equation. To evaluate the pressure, the divergence of the equation for the pressure substep is taken, and continuity is enforced at the completion of each timestep. More details on the general method and application to similar problems can be found in the following papers: Thompson *et al.*,[43] Griffith *et al.*,[44] Stewart *et al.*,[45] and Thompson, Leweke, and Provansal.[46]

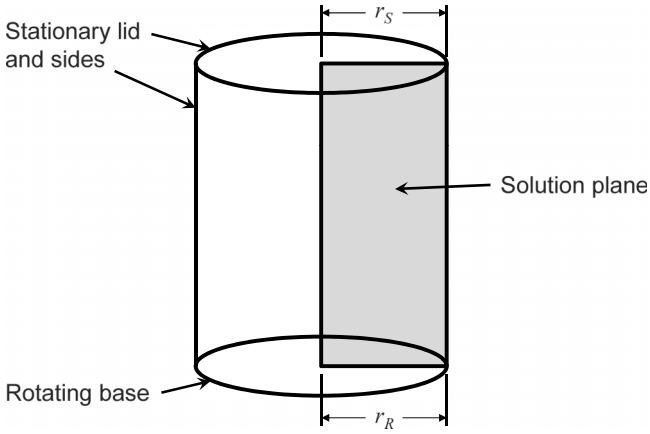

FIG. 1. TDC geometry.

III. SETUP AND VALIDATION

A. The TDC

A schematic of the TDC is presented in Figure 1. We initially define the Reynolds number Re in the usual manner based on the cylinder rotating base radius r_R, the angular velocity of the lid $\dot{\Theta}$, and the kinematic viscosity ν,

$$Re = \frac{\dot{\Theta} r_R^2}{\nu}. \tag{1}$$

The aspect ratio (Ar) is defined as the cylinder height/radius ratio.

For the Reynolds numbers considered, the flow has been shown in the previous work to be axisymmetric.[47,48] (As mentioned earlier, due to small geometrical imperfections and dye visualisation inaccuracies, in practice, an asymmetric open bubble can sometimes be observed in experiments, as described by Thompson and Hourigan,[32] Brøns *et al.*,[33] and Brøns, Thompson, and Hourigan.[35])

Assuming axisymmetry, we model only a single plane which includes the axis of the cylinder, as shown in Figure 1. For the steady spectral-element simulations, the grid adjacent to all walls including the axis was compressed in the wall-normal direction, in order to accurately capture the stationary wall boundary layers and the Ekman layer above the rotating lid. All of the solutions were converged to machine accuracy. The grid used 50×20 cells and each cell is further subdivided into $N \times N$ internal nodes.Table I shows the predicted critical Reynolds number for the onset of breakdown and the axial location of breakdown z_b for the 2.5 aspect ratio TDC as a function of the internal element resolution. Clearly, there is negligible difference between the $N = 4$ and $N = 5$ predictions. The simulation results reported in this paper used $N = 4$ elements.

In Figure 2, we compare with experimental results for a TDC with aspect ratio 2.5 over a range of Reynolds numbers. Although there are slight differences (see Table II), these are likely to be a result of uncertainties in the experimental setup, and especially in the determination of the viscosity,

TABLE I. Convergence study showing the predicted critical Reynolds number for the onset of breakdown in a 2.5 aspect ratio TDC as a function of macro-element internal nodes. The % deviations indicate the differences from the finest grid result ($N = 5$).

N	Re_{crit}	z_b	% deviation of Re_{crit}
3	1905.219	0.766 145	0.03
4	1904.580	0.768 651	0.0001
5	1904.578	0.768 650	⋯

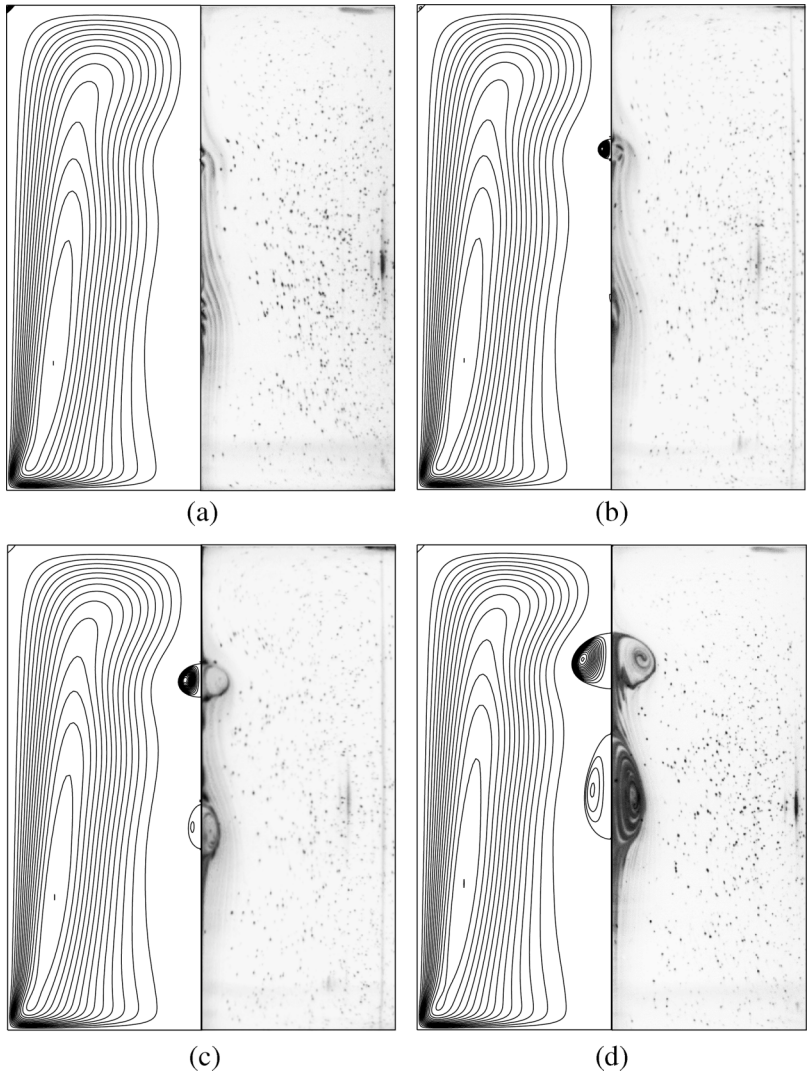

FIG. 2. Numerical versus experimental results for (a) $Re = 1902$, (b) $Re = 1933$, (c) $Re = 2001$, and (d) $Re = 2252$. Experimental dye visualisation taken at the CSIRO by Dr. L. Graham (see Hourigan, Graham, and Thompson[34] for description of technique). Reprinted with permission from Hourigan *et al*. Phys. Fluids **7**, 3126–3128 (1995). Copyright 1995 American Institute of Physics.

as described in Hourigan, Graham, and Thompson,[34] for which the bubble dimensions are very sensitive. Despite these small differences, these comparisons further validate the simulations.

B. The open pipe

The pipe geometry is based on that used in the experiments of Faler and Leibovich,[49] and is shown in Figure 3.

TABLE II. Breakdown bubble location: difference between the simulations and experimental dye visualisations.

Re	1933	2001	2252
Difference	3.0%	0.0%	0.0%

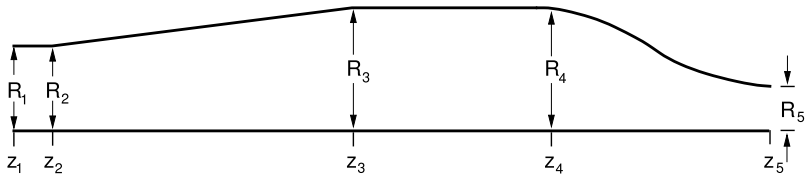

FIG. 3. Pipe geometry from Faler and Leibovich.[49] The relative dimensions are $R_1 = R_2 = 1.0$, $R_3 = R_4 = 1.333$, $R_5 = 0.667$; $z_1 = 0$, $z_2 = 1$, $z_3 = 14$, $z_4 = 21.87$, $z_5 = 32.37$.

In order to allow the flow to develop without any imposed symmetries, we conduct simulations using the three-dimensional spectral/spectral-element solver. Inlet swirl and axial velocity profiles are described by functions fitted to the velocity profiles measured upstream of breakdown in the experiment of Faler and Leibovich,[49]

$$u = \frac{1 + \beta e^{-\alpha r^2}}{1 + \beta},$$
$$w = \zeta \frac{\gamma}{r}(1 - e^{-\alpha r^2}).$$

Here, $\alpha = 11.84$, $\beta = 1.4376$, $\gamma = 0.304\,15$, and $\zeta = 1$.

The swirl is varied by varying the scaling factor ζ in the equation for the swirl velocity. Both the Reynolds number and swirl are varied simultaneously in order to provide solutions with breakdown.

Calculations were performed on a 10×324 element mesh (using 5×5 elements), with 64 Fourier planes. Calculations comparing results from 5×162 and 10×324 meshes with the steady axisymmetric spectral-element code resulted in a change in the predicted critical Reynolds number for axisymmetric breakdown of approximately 0.1% at $Re = 1280$, hence the results for the three-dimensional $10 \times 324 \times 64$ mesh should be well resolved.

IV. INITIAL COMPARISON OF THE PIPE AND TDC FLOWS

We initially compare breakdown in the open pipe and TDC flows. Since the spiral is not observed in the TDC (a possible reason for this is suggested later), at present, we focus on axisymmetric bubble breakdown. We begin with the obvious initial observation that the bubbles in the TDC resemble in a number of fundamental ways the bubbles produced in pipes (see, e.g., Faler and Leibovich[49] and Sarpkaya[50]). There is a stagnation point on the axis, followed by a substantially axisymmetric region of recirculation. At low *Re*, the observations by Sarpkaya[50] of the bubble form in the pipe match closely images of the bubble in the TDC, although Leibovich[51] notes that there is some asymmetry at the downstream end of the bubbles. As pointed out previously, this asymmetry is also seen in the TDC, but this is due to geometrical imperfections (albeit small), numerical grid periodicities,[32,33] or even dye injection offsets and diffusion.[34,35] This may also be the case for predominantly axisymmetric bubbles in pipes before true spiral breakdown is triggered.

Similarities can also be seen in the velocity profiles of the flows upstream of breakdown, shown in Figure 4. The inlet axial (u) and azimuthal (w) velocity profiles obtained by Faler and Leibovich[52] for $Re = 2560$ are shown on the left in Figures 4(a) and 4(c), alongside the equivalent plots (right) for the TDC for $Re = 1933$, just upstream of breakdown. Close to the axis, both axial velocity profiles are jet-type, and the azimuthal (swirl) velocity profiles are roughly solid-body.

V. CONSISTENT PARAMETERS FOR DEFINING BREAKDOWN SUSCEPTIBILITY

Swirl strength is fundamental to the susceptibility of the flow to breakdown, and in the literature, various definitions exist. Some studies use the ratio of the maximum azimuthal velocity[53] or circulation[24] to the freestream axial velocity. Harvey[54] used the maximum swirl angle. Vaidya *et al.*[55] used the "swirl intensity," the azimuthal mass flux divided by the axial mass flux.

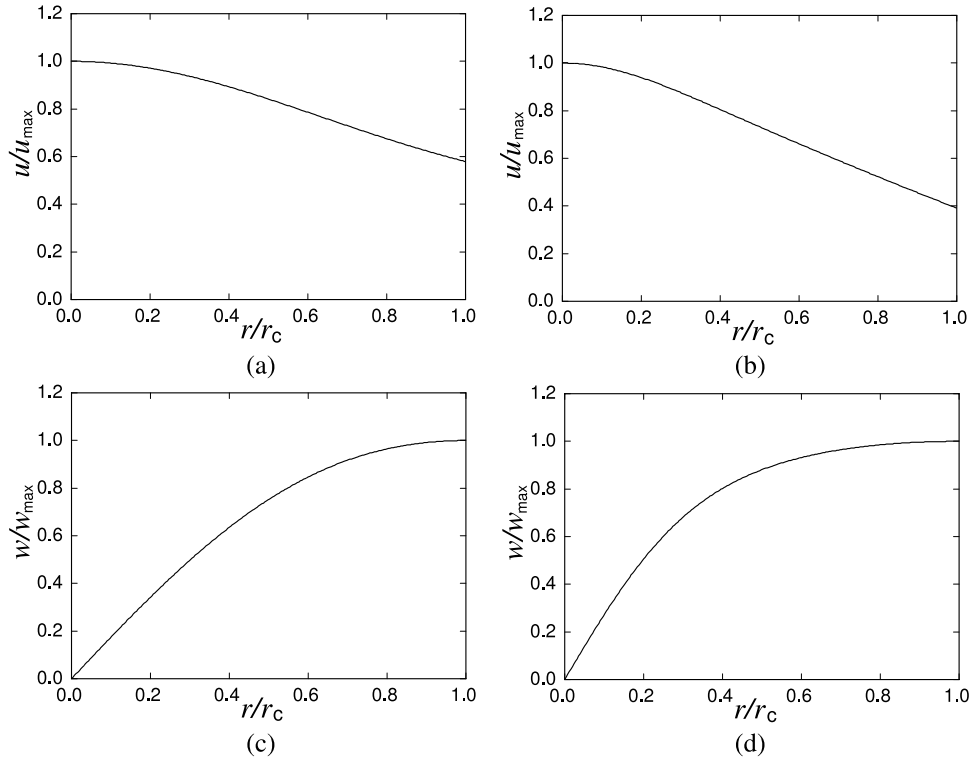

FIG. 4. ((a) and (b)) Normalized axial velocity u and ((c) and (d)) normalised swirl velocity w profiles upstream of breakdown for the pipe from Faler and Leibovich[52] ($Re = 2560$, $\Omega = 1.777$), left, and the TDC ($Re = 1933$), right. (a) F&L (b) TDC (c) F&L (d) TDC.

All of these definitions (with the possible exception of that of Harvey[54]) include one or more quantities that represent the flow outside the vortex core. In the current work, we suggest a definition that describes the characteristics of the vortex core only. Since the nature of the vortex core, rather than the external flow, is presumably fundamental to the onset of breakdown, we suggest that this allows a better description of the susceptibility of the flow to breakdown. Also, since consideration of the external geometry is excluded, the definitions can be applied to both the open pipe and TDC geometries, and allow direct comparison of these two flows, which is the purpose of the current study.

We first define the following quantities:

1. u_{max}, the maximum axial velocity (positive in the flow direction, and upstream of breakdown if breakdown is present);
2. w_{max}, the maximum azimuthal velocity on a line, extending radially from the axial location of u_{max};
3. r_c, the radial location of w_{max} (r_c defines the vortex core radius).

We can then define Re' and Ω' by

$$Re' = \frac{u_{max} r_c}{\nu}, \tag{2}$$

$$\Omega' = \frac{w_{max}}{u_{max}}. \tag{3}$$

These definitions are not new; as mentioned above, the maximum azimuthal velocity has previously been used to define the level of swirl in the vortex core, and the radius of the vortex core has also previously been defined as the point at which the azimuthal velocity becomes a maximum. The novelty will lie in the use of these definitions for flows where they are not readily applied, in the present case for flow in the TDC.

TABLE III. Typical Re' and Ω' values for the TDC.

TDC Re	Breakdown state	Re'	Ω'
1902	No bubble	59.7	0.874
1933	1 bubble	59.8	0.890
2001	2 bubbles	60.3	0.930
2252	2 bubbles	61.3	1.121

The values of Re' and Ω' determined for the TDC for the cases shown in Figure 2 are presented in Table III. We first note the very low Re' compared with Re. Amongst other things, this is an indication of the relatively small velocity magnitudes in the breakdown bubbles of the TDC. In addition, Re' is almost constant with Re, while Ω' increases roughly linearly with Re.

These observations are true in general for TDC breakdown. Figure 5 shows the variation of these parameters in the neighbourhood of breakdown for aspect ratios in the range ($1.5 \leq Ar \leq 3.5$). Note that above $Ar \simeq 3.5$, time-dependent axisymmetric breakdown occurs prior to steady breakdown,[47,48] while the lower aspect ratio limit for breakdown is $Ar \simeq 1.2$.[48] Thus, this aspect ratio range approximately covers the aspect ratio limits for steady axisymmetric breakdown for the TDC. Importantly, this figure demonstrates that the effective Reynolds number is restricted to $Re' \lesssim 80$ for breakdown in the TDC.

The same parameters for the pipe are shown in Table IV. The Reynolds numbers are typical of those used in open pipe studies, e.g., Darmofal and Murman[24] ($Re = 1000$), Faler and Leibovich[52] ($Re = 2560$). Comparing results in the two tables, it can be seen that the Re' regimes at which breakdown is observed in the two geometries are quite different. Although the often-quoted Re for the TDC, based on the lid rotation rate, appears similar to the typical pipe flow Re, with respect to breakdown, the actual Re' is much lower in the TDC. This reduced Re' appears to account for the different manifestations of breakdown in the two geometries, as will be argued later.

Also, for the pipe, breakdown appears at a significantly lower Ω'. The reason for this is that as Re' decreases, the value of Ω' required for breakdown tends to increase (this point is confirmed in Sec. VII).

For the pipe, it is possible to independently control Re' and Ω' to explore a specific region in Re'/Ω' space. However, for a regular TDC with only the aspect ratio and lid rotation rate to vary, independent control of Re' and Ω' is difficult. This has implications for the observations of breakdown in the TDC. We suggest, for example, that the absence of the spiral and double helix modes of breakdown in the TDC is a result of the fact that for the simple TDC configuration, it is not possible to visit the part of Re'/Ω' space where these types of breakdown appear.

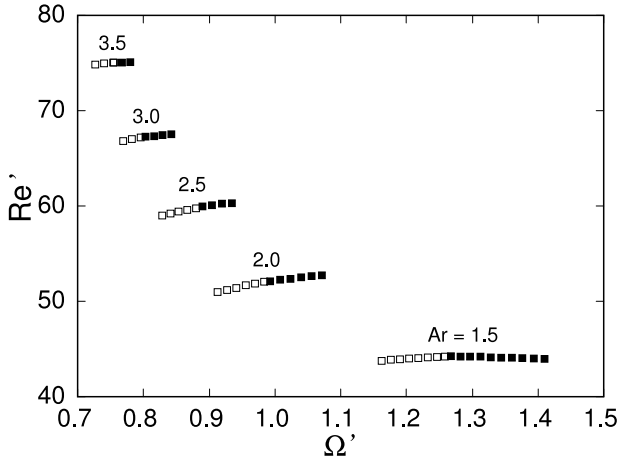

FIG. 5. Variation of Re' with Ω' in the neighbourhood of breakdown for the TDC. The aspect ratio is marked. Open squares—no breakdown, black squares—breakdown.

TABLE IV. Typical Re' and Ω' values for breakdown in the pipe of Faler and Leibovich.[52]

Pipe	Re	Ω	Breakdown state	Re'	Ω'
F&L	2560	1.0	Spiral	832	0.574
F&L	1280	1.0	Spiral	416	0.588

VI. BREAKDOWN VARIATION BETWEEN GEOMETRIES AND THE CLASSIFICATION OF BREAKDOWN

The vortex breakdown observed in open pipes and over delta wings has been characterised as a jump transition of the entire steady flow to another steady flow state.[56] It is difficult to reconcile the gradual transformation from parallel streamline flow to progressive streamline expansion and eventual development of a stagnation point and recirculation region in the TDC (Figure 2) with this picture of breakdown.

However, in Sec. V, the very different Re'/Ω' regimes normally occupied by the pipe and TDC flows were highlighted, and at sufficiently low Reynolds number, the gradual transition to breakdown in the open pipe does resemble that observed in the TDC.

The difference in Re'/Ω' regime also potentially provides an explanation for the absence of the spiral form of breakdown in the TDC. We propose that the reason for the lack of a (completely) axisymmetric bubble, and prevalence of the spiral form in the pipe, is the comparatively much higher Re' at which pipe studies are conducted. The higher effective Reynolds number means that viscous damping is lower, perhaps allowing spiral modes to be amplified. Experimentally, it would be very difficult to obtain results in the pipe for the Re' and Ω' values that result in breakdown in the TDC. However, it is a relatively simple matter to investigate these flows numerically. This will be undertaken in Sec. VII.

VII. THREE-DIMENSIONAL SIMULATION OF THE PIPE FLOW

To test the hypothesis that the spiralling asymmetry in the pipe is due to the high Reynolds numbers normally used, we examine solutions for decreasing Reynolds number and observe whether the flow (with breakdown) subsequently becomes axisymmetric. As expected, decreasing Reynolds number led to an increase in the amount of swirl necessary for breakdown.

Some three-dimensional solutions are visualised in Figure 6.

As Re' decreases, the three-dimensionality that is present from $Re' = 832$ to $Re' = 208$ completely disappears by $Re' = 104$. In addition, at $Re' = 104$, the bubble resembles much more closely the type of bubble observed in the TDC; the downstream end of the bubble has become closed. (This trend can also be inferred from computations by Ruith *et al.*[58] where, at constant swirl, increase in Re from $Re = 100$ to $Re = 300$ resulted in a transition from axisymmetric bubble to spiral, then finally to double helix breakdown.)

For $Re' = 104$ and $Re' = 52$, the bubble manifests very close to the inlet—compare this with the TDC, where breakdown also settles close to the upstream TDC wall. This type of breakdown would be difficult to produce in the pipe experimentally because it would be difficult to constrain within the test section; in our case, the bubble is fixed by the inlet boundary condition. Hence, the absence of the completely axisymmetric breakdown form (with no downstream spiral form) in open pipe experiments is not unexpected.

Re' and Ω' values for the three-dimensional pipe are plotted in Figure 7 along with values for the TDC at various Reynolds numbers and aspect ratios. In addition, for the open pipe, the dotted line shows the transition from no breakdown (at low swirl) to breakdown (at high swirl), for steady axisymmetric breakdown. Those results are obtained from the steady axisymmetric solver.

It can be seen from this plot that with decreasing Re' in the open pipe, the Ω' required for breakdown increases, until at the Re' where TDC breakdowns appear, the values of Ω' nearly match. Hence, with decreasing Reynolds number, there is a gradual transition from the open spiral type

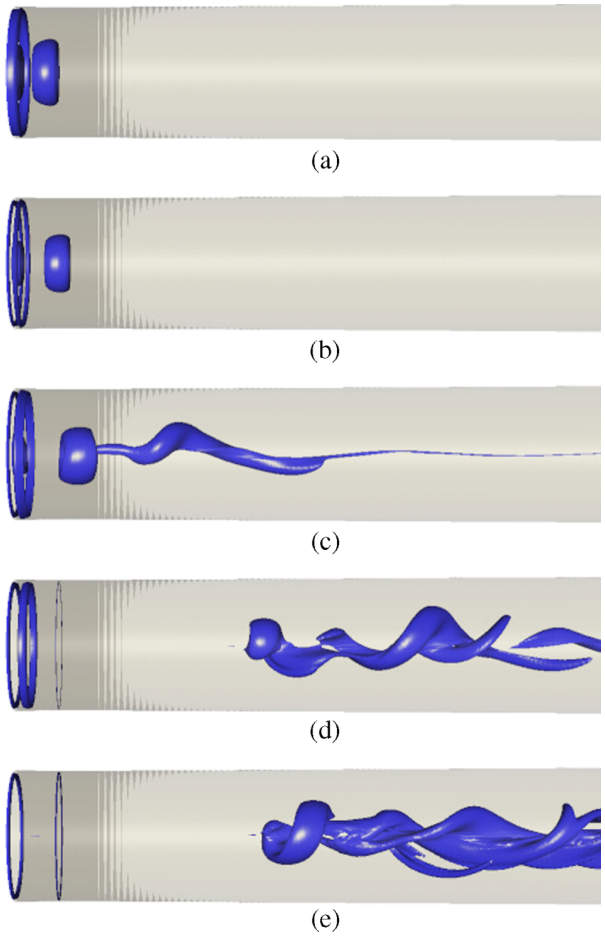

FIG. 6. Results for (a) $Re' = 832$, $\Omega' = 0.668$, (b) $Re' = 416$, $\Omega' = 0.668$, (c) $Re' = 208$, $\Omega' = 0.793$, (d) $Re' = 104$, $\Omega' = 0.919$, and (e) $Re' = 52$, $\Omega' = 1.169$. To visualize the vortical structures, we plot the region where the median eigenvalue λ_2 of the term $S^2+\Omega^2$ is negative, where S and Ω are the symmetric and antisymmetric parts of the velocity gradient tensor (Jeong and Hussain[57]).

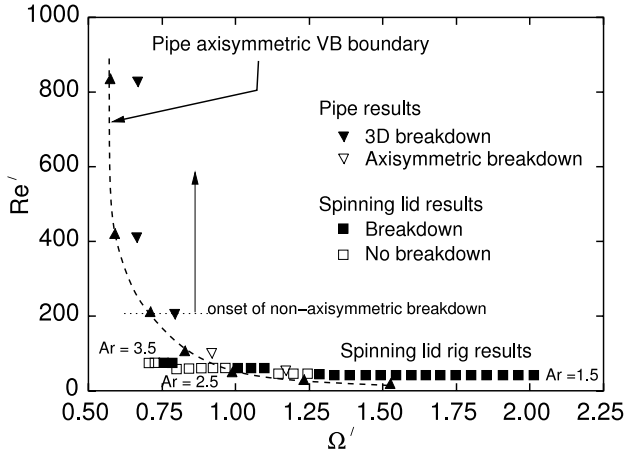

FIG. 7. Re' versus Ω' for the TDC (breakdown: □, no breakdown: ■), for the marked aspect ratios. Predictions for the open pipe geometry of Faler and Leibovich[52] are also shown. For the latter case, the dashed line with triangles (▲) indicates the transition curve for steady axisymmetric breakdown obtained from an axisymmetric solver (left: no breakdown, right: breakdown). In addition, inverted triangles show points corresponding to full 3D time-dependent simulations at which breakdown was observed to occur: axisymmetric steady breakdown (▽); non-axisymmetric unsteady breakdown (▼).

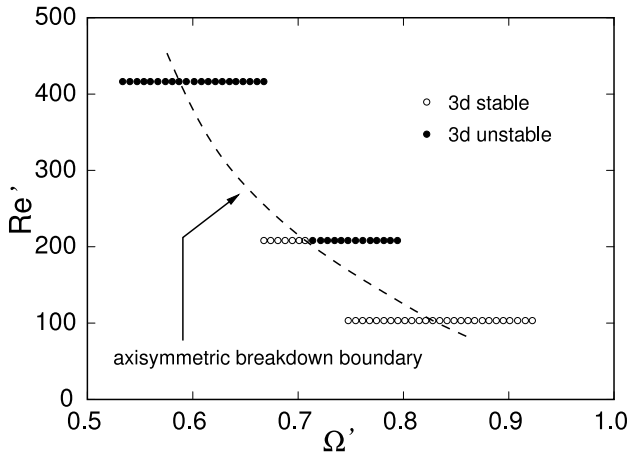

FIG. 8. Stability of steady axisymmetric flow state to three-dimensional perturbations for the pipe geometry of Faler and Leibovich.[49]

breakdown often observed in pipe experiments, to a closed bubble axisymmetric breakdown more commonly associated with the TDC.

To investigate the onset of non-axisymmetric unsteady breakdown further, unsteady three-dimensional simulations were performed using the steady axisymmetric flow state as an initial condition, for different Reynolds numbers over a range of swirl parameter values. This initial velocity field was perturbed with low-level white noise. The solutions were then evolved in time to investigate whether the perturbations would grow or decay, thus determining whether the steady axisymmetric flow state was stable or unstable. The results are shown in Figure 8.

At the lowest Reynolds number tested of $Re' = 104$, the steady axisymmetric flow is stable for the range of Ω' investigated, whilst at the highest Reynolds number ($Re' = 416$), the axisymmetric state is unstable even prior to axisymmetric breakdown. Hence, for the latter case, the axisymmetric breakdown state will not be observable. Interestingly, at the intermediate Reynolds number tested ($Re' = 208$), the flow remains stable to non-axisymmetric perturbations up to the first occurrence of the axisymmetric breakdown state at $\Omega' = 0.71$, but becomes unstable to non-axisymmetric perturbations just beyond this swirl ratio. Thus, this is approximately the highest Reynolds number at which the initial breakdown state can be steady and axisymmetric. A clear interpretation in this case is that spiral breakdown is a global instability of the axisymmetric breakdown state, consistent with the findings of Gallaire *et al.*,[27] and Meliga, Gallaire, and Chomaz.[28] Importantly, relevant to the main premise of this paper, Figure 5 indicates that the largest Reynolds number observed for the TDC is restricted to be less than 100. Thus, it is not surprising that the spiral breakdown state is not observed in the TDC because the flow state occupies a distinctly different region of (Re', Ω') parameter space.

VIII. CONCLUSIONS

The application of more consistent definitions for two primary parameters governing breakdown, Reynolds number, and swirl, based on the characteristics of the vortex core, enables a more meaningful and consistent comparison to be made between open pipe and TDC flows. In particular, TDC and open pipe flows typically studied have been shown to inhabit very different regions of (Re', Ω') parameter space. This observation is put forward as an explanation for the lack of three-dimensionality in the breakdown states of TDC flows.

As a test of this claim, the Reynolds number in a three-dimensional pipe simulation was progressively reduced towards the levels of those found in typical TDC breakdown flows, with the result that steady axisymmetric bubbles with the characteristics of TDC type breakdown were observed. In addition, an investigation of the stability of the axisymmetric flow states indicated that

they become stable to non-axisymmetric perturbations as the Reynolds number is lowered, leaving the axisymmetric state as the first occurring breakdown state in the part of (Re', Ω') parameter space covered by TDC breakdown.

These observations, along with others outlined in this paper, confirm that as the Reynolds number for pipe flow is reduced, the open spiral mode of breakdown commonly observed in pipes is replaced by a closed axisymmetric bubble breakdown of the type observed in the TDC.

ACKNOWLEDGMENTS

The authors gratefully acknowledge the funding from Australian Research Council Discovery Grant (No. DP0452664) and Linkage International Grant (No. LX0668992) for supporting this research. Dr. Lachlan Graham of the Commonwealth Scientific and Industrial Research Organisation, Melbourne, is thanked for his flow visualisation photographs.

[1] I. Gursul, R. Gordnier, and M. Visbal, "Unsteady aerodynamics of nonslender delta wings," Prog. Aerosp. Sci. **41**, 515–557 (2005).
[2] J. Dusting, J. Sheridan, and K. Hourigan, "Flows within a cylindrical cell culture bioreactor with a free surface and a rotating base," in *Proceedings of the Fifteenth Australasian Fluid Mechanics Conference* (The University of Sydney, Sydney, Australia, 2004), ISBN 1-864-87695-6, CD-ROM.
[3] J. Dusting, J. Sheridan, and K. Hourigan, "A fluid dynamics approach to bioreactor design for cell and tissue culture," Biotechnol. Bioeng. **94**(6), 1196–1208 (2006).
[4] P. Yu, T. S. Lee, Y. Zeng, and H. T. Low, "Effects of conical lids on vortex breakdown in an enclosed cylindrical chamber," Phys. Fluids **18**, 117101 (2006).
[5] P. Yu, T. S. Lee, Y. Zeng, and T. H. Low, "Effect of vortex breakdown on mass transfer in a cell culture bioreactor," Mod. Phys. Lett. B **19**, 1543–1546 (2005).
[6] P. Yu, T. S. Lee, Y. Zeng, and H. T. Low, "Fluid dynamics of a micro-bioreactor for tissue engineering," Fluid Dyn. Mater. Process. **1**, 235–246 (2005).
[7] P. Yu, T. S. Lee, Y. Zeng, and T. H. Low, "Characterization of flow behaviour in an enclosed cylinder with a partially rotating end wall," Phys. Fluids **19**, 057104 (2007).
[8] P. Yu and S. A. Meguid, "Effects of wavy sidewall on vortex breakdown in an enclosed cylindrical chamber with a rotating end wall," Phys. Fluids **21**, 017104 (2009).
[9] K. Y. S. Liow, B. T. Tan, G. A. Thouas, and M. C. Thompson, "CFD modeling of the steady-state momentum and oxygen transport in a bioreactor that is driven by an aerial rotating disk," Mod. Phys. Lett. B **23**(2), 121–127 (2009).
[10] B. T. Tan, K. Y. S. Liow, L. Mununga, M. C. Thompson, and K. Hourigan, "Simulation of the control of vortex breakdown in a closed cylinder using a small rotating disk," Phys. Fluids **21**(2), 024104 (2009).
[11] G. Thouas, J. Sheridan, and K. Hourigan, "A bioreactor model of mouse tumor progression," J. Biomed. Bioeng. **2007**, 9.
[12] A. M. Mitchell and J. Delery, "Research into vortex breakdown control," Prog. Aerosp. Sci. **37**, 385–418 (2003).
[13] F. Gallaire, S. Rott, and J. M. Chomaz, "Experimental study of a free and forced swirling jet," Phys. Fluids **16**, 2907 (2004).
[14] E. J. Gutmark and S. A. Guillot, "Control of vortex breakdown over highly swept wings," AIAA J. **43**, 2065 (2005).
[15] Y. D. Cui, J. M. Lopez, T. T. Lim, and F. Marques, "Harmonically forced enclosed swirling flow," Phys. Fluids **21**, 034106 (2009).
[16] M. Z. Ismadi, P. Meunier, A. Fouras, and K. Hourigan, "Experimental control of vortex breakdown by density effects," Phys. Fluids **23**, 034104 (2011).
[17] P. Meunier and K. Hourigan, "Mixing in a vortex breakdown flow," J. Fluid Mech. **731**, 195–222 (2013).
[18] T. B. Benjamin, "Theory of the vortex breakdown phenomenon," J. Fluid Mech. **14**, 593–629 (1962).
[19] J. D. Randall and S. Leibovich, "The critical state: A trapped wave model of vortex breakdown," J. Fluid Mech. **58**, 495–515 (1973).
[20] S. Wang and Z. Rusak, "The dynamics of a swirling flow in a pipe and transition to axisymmetric vortex breakdown," J. Fluid Mech. **340**, 177–223 (1997).
[21] Z. Rusak, C. H. Whiting, and S. Wang, "Axisymmetric breakdown of a q-vortex in a pipe," AIAA J. **36**, 1848–1853 (1998).
[22] G. L. Brown and J. M. Lopez, "Axisymmetric vortex breakdown part 2. Physical mechanisms," J. Fluid Mech. **221**, 553–576 (1990).
[23] Z. Rusak, "Axisymmetric swirling flow around a vortex breakdown point," J. Fluid Mech. **323**, 79–105 (1996).
[24] D. L. Darmofal and E. M. Murman, "On the trapped wave nature of axisymmetric vortex breakdown," AIAA Paper No. 94-2318, 1994.
[25] P. Billant, J.-M. Chomaz, and P. Huerre, "Experimental study of vortex breakdown in swirling jets," J. Fluid Mech. **376**, 183–219 (1998).
[26] F. Gallaire and J.-M. Chomaz, "Mode selection in swirling jet experiments: A linear stability analysis," J. Fluid Mech. **494**, 223–253 (2003).
[27] F. Gallaire, M. Ruith, E. Meiburg, J. M. Chomaz, and P. Huerre, "Spiral vortex breakdown as a global mode," J. Fluid Mech. **549**, 71 (2006).
[28] P. Meliga, F. Gallaire, and J.-M. Chomaz, "A weakly nonlinear mechanism for mode selection in swirling jets," J. Fluid Mech. **699**, 216–262 (2012).
[29] Z. Rusak and D. Lamb, "Prediction of vortex breakdown in leading-edge vortices above slender delta wings," J. Aircr. **36**, 659–667 (1999).

[30] F. Renac and L. Jacquin, "Linear stability properties of lifting vortices over delta wings," AIAA J. **45**, 1942–1951 (2007).
[31] M. A. Herrada and R. Fernandez-Feria, "On the development of three-dimensional vortex breakdown in cylindrical regions," Phys. Fluids **18**, 084105 (2006).
[32] M. C. Thompson and K. Hourigan, "The sensitivity of steady vortex breakdown bubbles in confined cylinder flows to rotating lid misalignment," J. Fluid Mech. **496**, 129–138 (2003).
[33] M. Brøns, W. Z. Shen, J. N. Sørensen, and W. J. Zhu, "The influence of imperfections on the flow structure of steady vortex breakdown bubbles," J. Fluid Mech. **578**, 453–466 (2007).
[34] K. Hourigan, L. W. Graham, and M. C. Thompson, "Spiral streaklines in pre-vortex breakdown regions of axisymmetric swirling flows," Phys. Fluids **7**, 3126–3128 (1995).
[35] M. Brøns, M. C. Thompson, and K. Hourigan, "Dye visualization near a 3D stagnation point: Application to the vortex breakdown bubble," J. Fluid Mech. **622**, 177–194 (2009).
[36] F. Marques and J. M. Lopez, "Precessing vortex breakdown mode in an enclosed cylinder flow," Phys. Fluids **13**, 1679–1682 (2001).
[37] J. M. Lopez, "Rotating and modulated rotating waves in transitions of an enclosed swirling flow," J. Fluid Mech. **553**, 323–346 (2006).
[38] J. N. Sørensen, V. Naumov, and V. L. Okulov, "Multiple helical modes of vortex breakdown," J. Fluid Mech. **683**, 430–441 (2011).
[39] J. M. Lopez, "Three-dimensional swirling flows in a tall cylinder driven by a rotating endwall," Phys. Fluids **24**, 014101 (2012).
[40] O. C. Zienkiewicz, *The Finite Element Method*, 3rd ed. (McGraw-Hill, London, 1977).
[41] M. C. Thompson, K. Hourigan, and J. Sheridan, "Three-dimensional instabilities in the wake of a circular cylinder," Exp. Therm. Fluid Sci. **12**, 190–196 (1996).
[42] G. E. Karniadakis and G. Triantafyllou, "Three-dimensional dynamics and transition to turbulence in the wake of bluff bodies," J. Fluid Mech. **238**, 1–30 (1992).
[43] M. C. Thompson, K. Hourigan, A. Cheung, and T. Leweke, "Hydrodynamics of a particle impact on a wall," Appl. Math. Model. **30**, 1356–1369 (2006).
[44] M. D. Griffith, T. Leweke, M. C. Thompson, and K. Hourigan, "Pulsatile flow in stenotic geometries: Flow behaviour and stability," J. Fluid Mech. **622**, 291–320 (2009).
[45] B. E. Stewart, M. C. Thompson, T. Leweke, and K. Hourigan, "Numerical and experimental studies of the rolling sphere wake," J. Fluid Mech. **643**, 137–162 (2010).
[46] M. C. Thompson, T. Leweke, and M. Provansal, "Kinematics and dynamics of sphere wake transition," J. Fluids Struct. **15**, 575–586 (2001).
[47] J. M. Lopez, "Axisymmetric vortex breakdown part 1. Confined swirling flow," J. Fluid Mech. **221**, 533–552 (1990).
[48] M. P. Escudier, "Observations of the flow produced in a cylindrical container by a rotating endwall," Exp. Fluids **2**, 189–196 (1984).
[49] J. H. Faler and S. Leibovich, "Disrupted states of vortex flow and vortex breakdown," Phys. Fluids **20**, 1385–1400 (1977).
[50] T. Sarpkaya, "On stationary and travelling vortex breakdowns," J. Fluid Mech. **45**, 545–559 (1971).
[51] S. Leibovich, "Vortex stability and breakdown: Survey and extension," AIAA J. **22**, 1192–1206 (1984).
[52] J. H. Faler and S. Leibovich, "An experimental map of the internal structure of a vortex breakdown," J. Fluid Mech. **86**, 313–335 (1978).
[53] J. M. Delery, "Aspects of vortex breakdown," Prog. Aerospace Sci. **30**, 1–59 (1994).
[54] J. K. Harvey, "Some observations of the vortex breakdown phenomenon," J. Fluid Mech. **14**, 585–592 (1962).
[55] H. A. Vaidya, Ö. Ertunç, B. Genç, F. Beyer, Ç. Köksoy, and A. Delgado, "Numerical simulations of swirling pipe flows—decay of swirl and occurrence of vortex structures," J. Phys.: Conf. Ser. **318**, 1–10 (2011).
[56] M. Goldshtik and F. Hussain, "Analysis of inviscid vortex breakdown in a semi-infinite pipe," Fluid Dyn. Res. **23**, 189–234 (1998).
[57] J. Jeong and F. Hussain, "On the identification of a vortex," J. Fluid Mech. **285**, 69–94 (1995).
[58] M. R. Ruith, P. Chen, E. Meiburg, and T. Maxworthy, "Three-dimensional vortex breakdown in swirling jets and wakes: Direct numerical simulation," J. Fluid Mech. **486**, 331–378 (2003).